J. of Electromagn. Waves and Appl., Vol. 26, 468–479, 2012

FREQUENCY SCANNING ARRAY COMPOSED OF ANTIPODAL LINEARLY TAPERED SLOT ANTENNAS

R. Camblor*, S. Ver Hoeye, C. Vázquez, G. Hotopan, M. Fernández, and F. Las-Heras

University of Oviedo, Campus de Viesques 33203, Gijón/Xixón, Spain

Abstract—In this work, a frequency scanning array of antipodal linearly tapered slot antennas is presented. The system is capable of performing beam steering from −11 to 10 degrees while sweeping the frequency from 8.25 GHz to 11.5 GHz. The beam scanning is achieved by means of a specially designed feeding network that divides the power and introduces the proper phase shift for each antenna port in the frequency range of interest. Experimental results showing the full array behaviour are also presented.

1. INTRODUCTION

Electronic beam steering is an appreciated antenna quality because it allows recovering information from different spacial directions, leading to interesting applications [1, 2], without the necessity of a mechanical system to modify the direction of the antenna beam [3], resulting in a simpler, lighter, faster and more flexible system. To achieve this using a phased array antenna [4–8], different techniques based on the use of phase shifters [9], switches [10], Rotman lenses [11] or Butler matrices [12] can be utilized. The technique applied in the array here is frequency scanning [13, 14], i.e., the beam steering effect is achieved through a variation of the input frequency.

In a frequency scanning antenna, the variation of the frequency leads to a shift of the phase front. To accomplish the desired effect, it is necessary to design a feeding network that provides the appropriate frequency dependent phase difference between adjacent elements.

Received 22 December 2011, Accepted 23 January 2012, Scheduled 15 February 2012

* Corresponding author: Rene Camblor Diaz (rcamblor@tsc.uniovi.es).

2. SINGLE RADIATING ELEMENT

The frequency scanning technique requires a circuit matched all over the range of interest. To achieve this objective, Tapered Slot Antenna (TSA) is a very good option, due to its wide broadband behaviour. If a conventional TSA is fed using a microstrip line then the bandwidth decays because of the transitions between microstrip lines and slot lines, which are likely to be narrow-band if fabricated in a low dielectric constant substrate [15]. This drawback can be overcome using an antipodal TSA, since in this case the required transition is between a microstrip line and a balanced microstrip line, which does not limit the bandwidth if properly designed.

The tapering has been chosen to be linear for the easiness of design and implementation, although it is known that better directivities can be obtained using more complicated tapers, requiring more precise fabrication techniques [16, 17].

The main TSA characteristics basically depend on two variables: the element length and the taper geometry. The element width barely affects the antenna performance and thus provides design flexibility.

To obtain a more compact array configuration, the classical

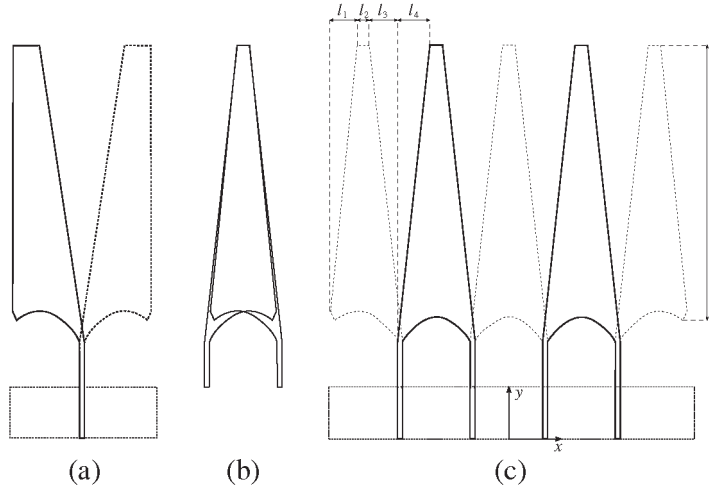

Figure 1. Schematic representations of different linearly tapered slot antennas. (a) Traditional linearly TSA. (b) Union of two traditional linearly TSA to form the double linearly TSA implemented in this work. (c) Array composed of double linearly TSA. Note that, for the sake of clarity, the dielectric is not represented and the dashed lines represent the bottom side of the dielectric.

antipodal linearly TSA has been modified in the following way: a half of a linearly TSA is fused with the same half, but after applying a specular symmetry along the longitudinal axis. The lengthways edges of the fused antenna are then cropped to taper both sides. By this operation, a double linearly TSA is obtained and it shall be fed using two microstrip ports. A scheme of the process followed to designed the double linearly TSA is presented in Figure 1. The length values referred are $l_1 = 8.5\,\text{mm}$, $l_2 = 3.93\,\text{mm}$, $l_3 = 18.1$ mm, $l_4 = 11.66\,\text{mm}$ and $l_5 = 117.7\,\text{mm}$. This configuration allows having more radiatiating elements in the same space, which leads to an improvement of the radiation diagram and prevents the appearence of grating lobes. Due to the symmetry presented by this configuration, a 180° phase shift is required between two adjacent ports in order to have a broadside radiation diagram.

3. FEEDING NETWORK

The simplest approach to design a beam steering antenna array is to feed different array elements with the same amplitude and a progressive phase distribution. Thus, the variation of phase difference between adjacent elements causes the desired beam steering effect. As comented in Section 2, the symmetry of the elements requires a 180° progressive phase distribution to produce a broadside radiation pattern. This fact must be taken into account while performing the design of the feeding network. The designed network is a frequency phase shifter and a power divider [18–21] from one input port to four output ports. The network is composed of sections of four different impedances: $30\,\Omega$, $40\,\Omega$, $60\,\Omega$ and $120\,\Omega$. Using these impedance values it is possible to design, neglecting propagation losses, a one input to four outputs power divider, where every output gets a quarter of the signal at the input. The $50\,\Omega$ input is connected to Section A by a line of $\sqrt{30 \cdot 40}\,\Omega$ which length has been optimized to maximize the return loss, see Table 1. While the impedance was used to the obtain the appropriate power division, the different radious of each section have been optimized to

Table 1. Geometrical properties of the feeding network.

Section	Length [mm]	Width [μm]	Impedance [Ω]
A	7.8	3712.4	30
B	27	2481	40
C	27	1295	60
D	27	254.2	120

provide the desired phase change. These lengths are one of the most important criteria to determine the distance between two adjacent elements of the array.

Figure 2 shows the scheme of the described feeding network. Port 1 is placed at the 50 Ω input of the network, meanwhile ports 2, 3, 4 and 5

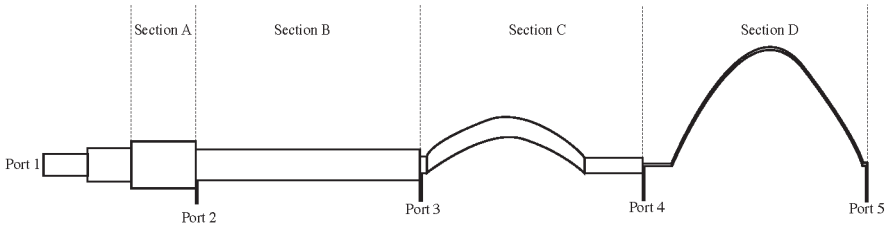

Figure 2. Scheme of the feeding network.

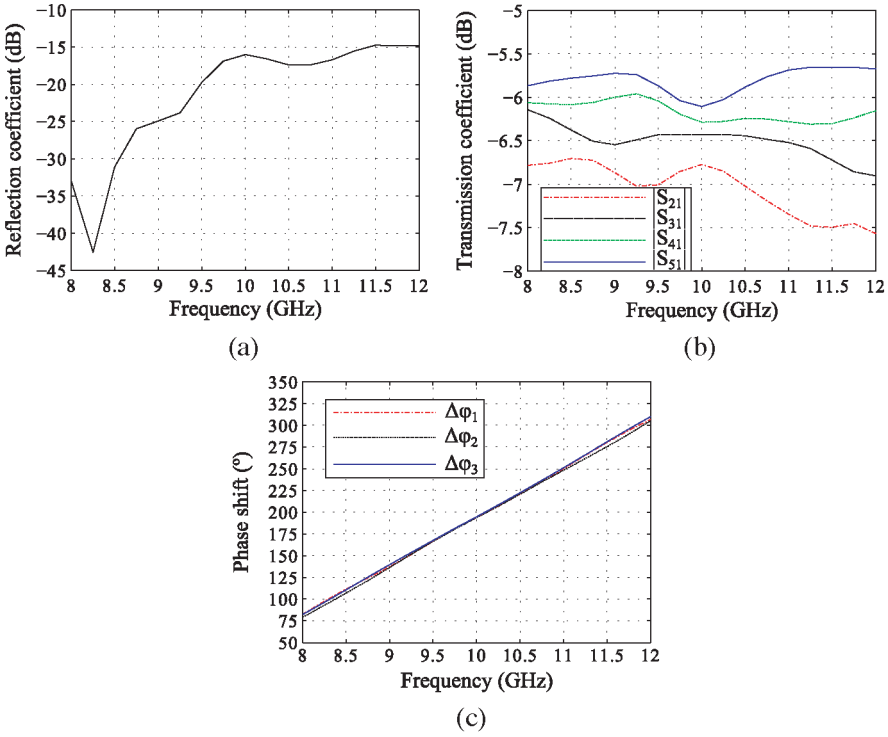

Figure 3. Simulated scattering parameters of the feeding line. (a) Amplitude of reflection coefficient at the input of the power divider. (b) Amplitude of the transmission coefficient for each port. (c) Phase shift between each pair of adjacent ports.

are located at the four 120 Ω outputs of the network that are used to feed the antenna array.

In Figure 3 the simulated behaviour of the feeding line is presented. $|S_{ij}|$ represents the amplitud of the scattering parameter and $\Delta\varphi_{ij}$ is defined by (1a)–(1c) where φ is the phase of the corresponding scattering parameter.

$$\Delta\varphi_1 = \varphi_{S_{21}} - \varphi_{S_{21}} \tag{1a}$$

$$\Delta\varphi_2 = \varphi_{S_{31}} - \varphi_{S_{31}} \tag{1b}$$

$$\Delta\varphi_3 = \varphi_{S_{41}} - \varphi_{S_{41}} \tag{1c}$$

4. ARRAY CONFIGURATION

To obtain the desired radiation diagram the Double TSA presented in Section 2 shall be used in pairs or in groups. In this configuration adjacent elements must be placed in different sides of the substrate. Finally the array is terminated using a half of the Traditional TSA on each corresponding side of the substrate so that it matches properly with its contiguous Double TSA. The distance in between adjacent antennas is 27 mm. All the elements are fed by the network described in Section 3. Due to the intrinsic characteristics of the TSA, the array has linear polarization in the substrate plane.

The surface current distribution of an array composed of a Double TSA and two halves of a Traditional TSA is shown in Figure 4, for the operation frequency of 10 GHz.

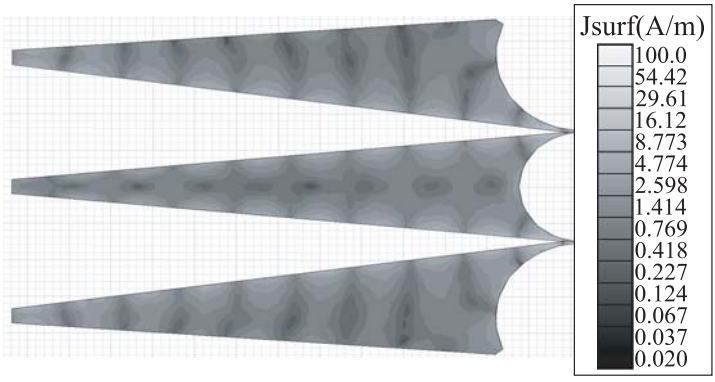

Figure 4. Surface current distribution on the conductors of a three element array. Note that, for the sake of clarity, the dielectric is not represented. The central antenna is on the bottom side of the dielectric, while the single port antennas are on the top side of the dielectric.

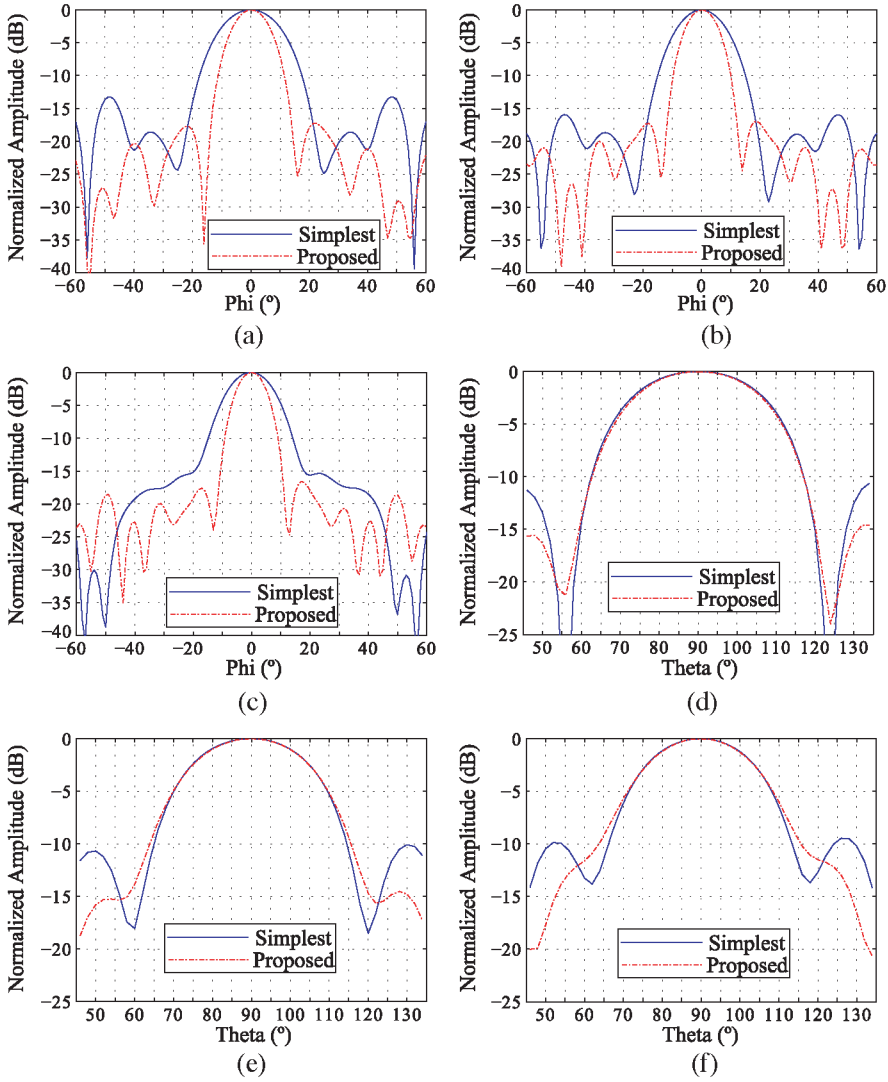

Figure 5. Simulated copolar radiation diagrams for the simplest array with a double linearly TSA and for the array proposed. Note that all diagrams are normalized. (a) E plane at 9 GHz. (b) E plane at 10 GHz. (c) E plane at 11 GHz. (d) H plane at 9 GHz. (e) H plane at 10 GHz. (f) H plane at 11 GHz.

Figure 5 shows a comparison between the the simplest array with a double linearly TSA (Figure 4) and the one proposed (Figure 1(c)). The arrays have not been fed using the feeding network that provides

the phase shift, but the required microstrip ports with constant phase. The effect of the array factor is clearly seen for the copolar E plane pattern. The a-symmetry between the top and the bottom sides of the array barely affects the symmetry of the H plane pattern.

5. EXPERIMENTAL RESULTS

The structures have been implemented on the 765 μm thick Arlon 25 N substrate, with $\varepsilon_r = 3.38$ and $\tan\delta = 0.0025$ at 10 GHz. The whole radiation system formed by the array of linearly tapered slot antennas and the power divider (Figure 6) has been optimized in order to be matched for the input port in the 8.25–12 GHz frequency band, this

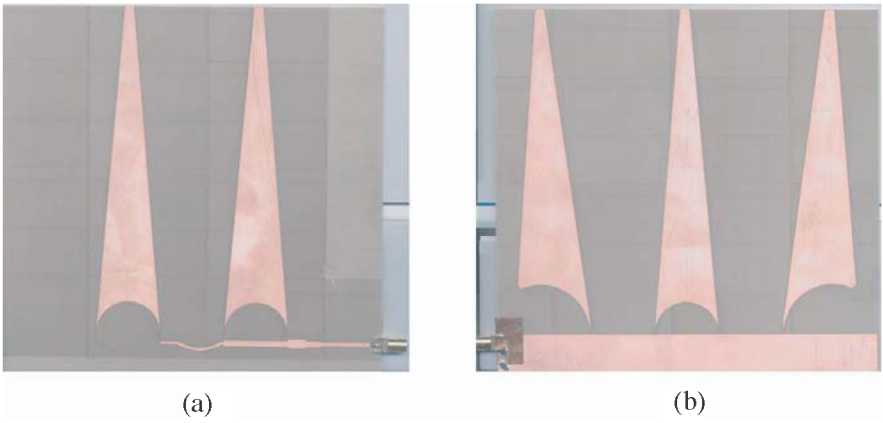

Figure 6. Photograph of both sides of the manufactured array. (a) Top side. (b) Bottom side.

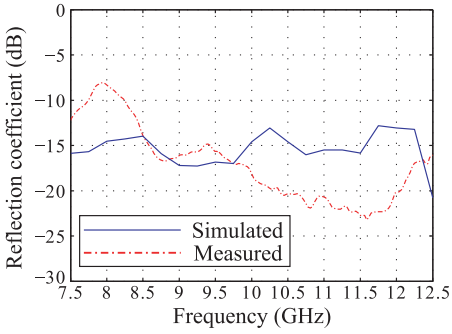

Figure 7. Measured amplitude of the reflection parameter of the complete frequency scanning system, i.e., feeding network and antenna.

being 40% of the central frequency. As shown in Figure 7, the measured return loss is consistent with the simulated one. The experimental radiation diagrams are close to those simulated using a finite element method (FEM) software. The dissimilarities are due to the precision limits of the machinery used, which causes small differences between the manufactured and the designed power divider. Also the issue of attaching the antenna to the measurement device of the anechoic

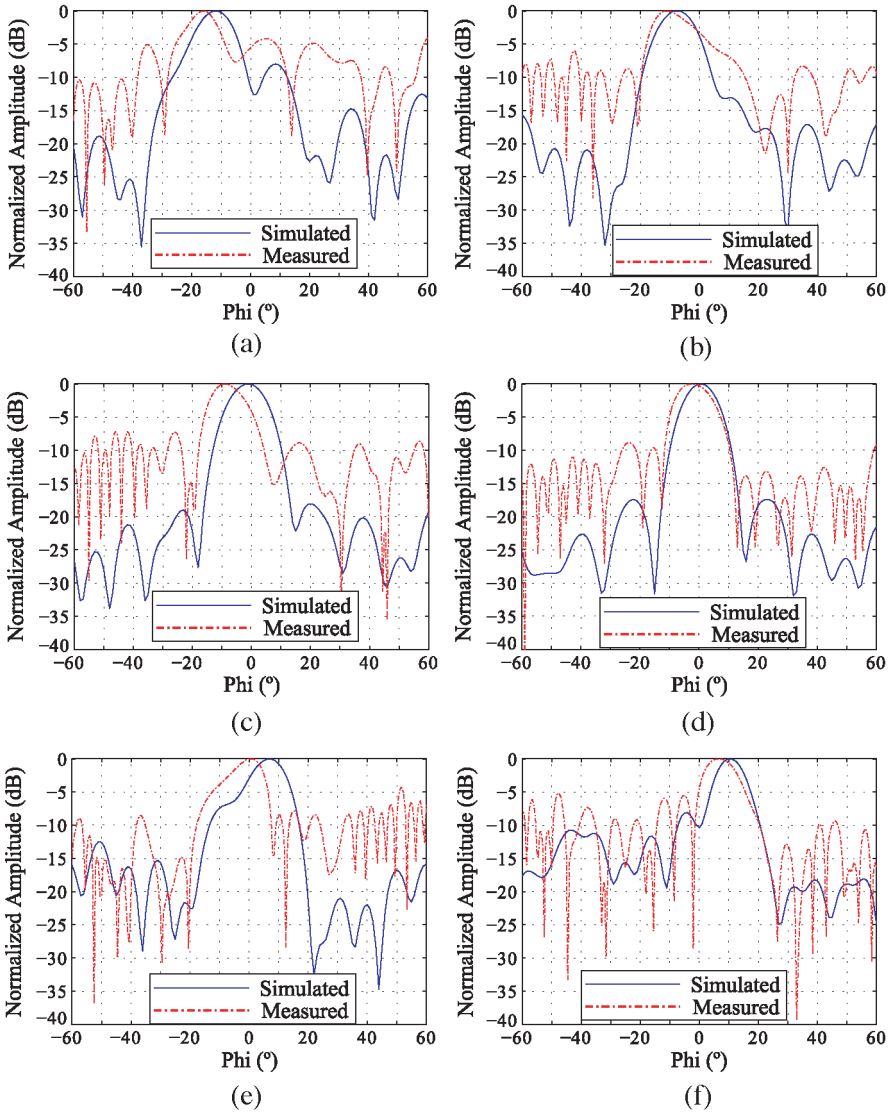

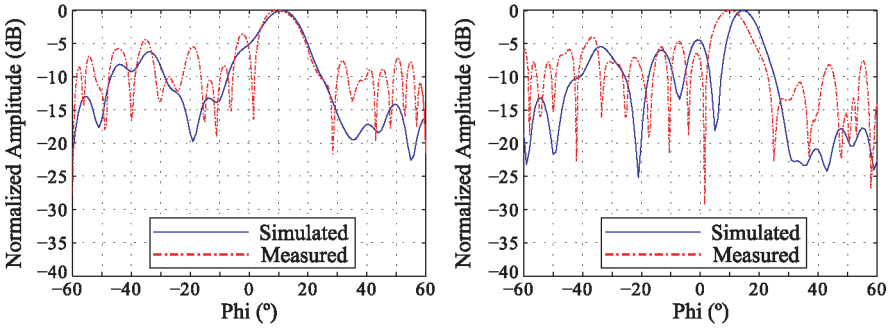

Figure 8. Simulated and measured copolar E plane radiation diagrams of the antenna. Note that all diagrams are normalized. (a) 8 GHz. (b) 8.25 GHz. (c) 9 GHz. (d) 9.25 GHz. (e) 10 GHz. (f) 10.75 GHz. (g) 11 GHz. (h) 11.5 GHz.

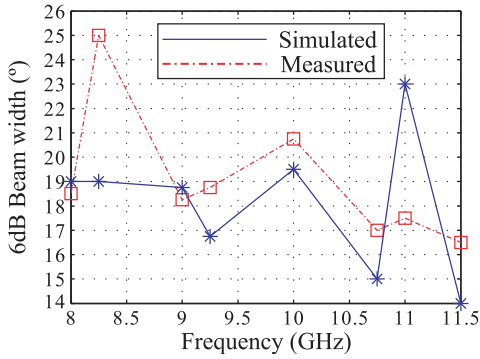

Figure 9. Measured 6 dB beam width. The figure has been elaborated using the data of the copolar E plane.

chamber may cause some differences. The copolar E plane diagrams show that the antenna is beam scanning capable in the substrate plane. Sweeping the frequency from 8.25 GHz to 11.5 GHz provides a change in the beam pointing angle from $\phi = -11°$ to $\phi = 10°$, i.e., 21° of continuous beam steering with a frequency sweep of 2.75 GHz, see Figure 8. In Figure 9 it is shown that the frequency scanning does not affect significantly the 6 dB beam width, which is for most of the measurements under 20°. On the other hand, the maximum of the copolar H plane diagram is always in the same position, independently of the frequency sweep, see Figure 10. Note that the axes shown in Figure 1(c) represent the coordinate system used in all radiation diagrams.

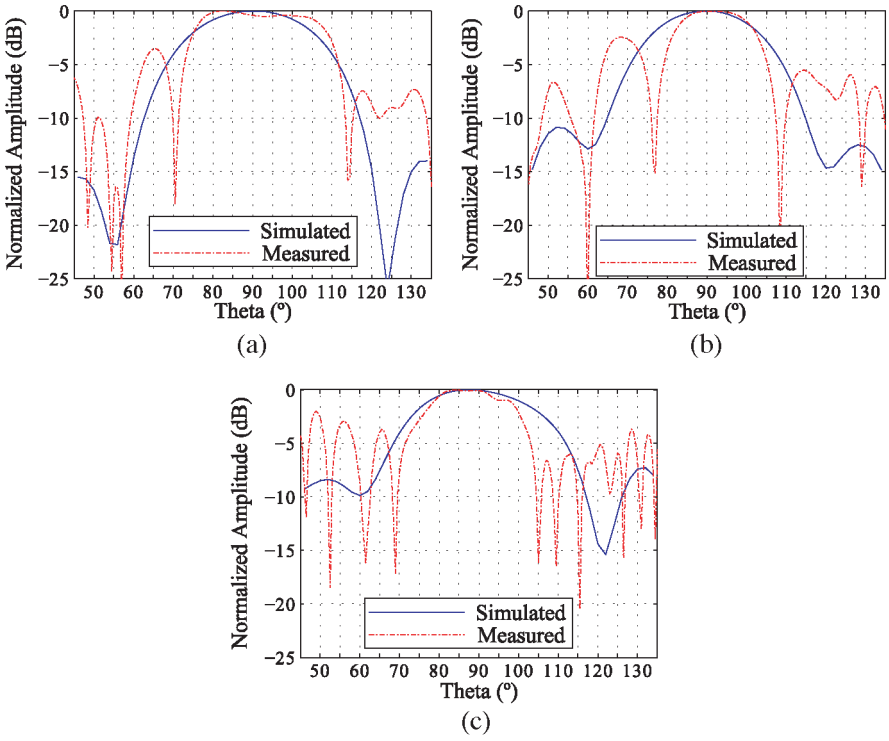

Figure 10. Simulated and measured copolar H plane radiation diagrams of the antenna. Note that all diagrams are normalized. (a) 9 GHz. (b) 10 GHz. (c) 11 GHz.

6. CONCLUSIONS

A frequency scanning system has been presented, composed of an array of novel double linearly tapered slot antennas and a feeding network that performs the power division and provides the proper phase shift between adjacent elements. A 21° change in the beam pointing angle is achieved by sweeping the frequency from 8.25 GHz and 11.5 GHz.

ACKNOWLEDGMENT

This work has been supported by the "Ministerio de Ciencia e Innovación" of Spain/FEDER under projects TEC2008-01638/TEC, IPT-2011-0951-390000 and CONSOLIDER-INGENIO CSD2008-00068 and grant AP2009-0438, by the Gobierno del Principado de Asturias (PCTI)/FEDER-FSE under projects EQUIP08-06, FC09-COF09-12,

EQUIP10-31 and PC10-06, grant BP10-031 and by Cátedra Telefónica-Universidad de Oviedo.

REFERENCES

1. Zhong, X. J., T. J. Cui, Z. Li, Y. B. Tao, and H. Lin, "Terahertz-wave scattering by perfectly electrical conducting objects," *Journal of Electromagnetic Waves and Applications*, Vol. 21, No. 15, 2331–2340, 2007.
2. Zhang, Z. and W. Dou, "A compact THz scanning imaging system based on improved reverse-microscope system," *Journal of Electromagnetic Waves and Applications*, Vol. 24, Nos. 8–9, 1045–1057, 2010.
3. Dou, W.-B., H. F. Meng, B. Nie, Z.-X. Wang, and F. Yang, "Scanning antenna at THz band based on quasi-optical techniques," *Progress In Electromagnetics Research*, Vol. 108, 343–359, 2010.
4. Yuan, H.-W., S.-X. Gong, P.-F. Zhang, and X. Wang, "Wide scanning phased array antenna using printed dipole antennas with parasitic elements," *Progress In Electromagnetics Research Letters*, Vol. 2, 187–193, 2008.
5. Oliveri, G. and L. Poli, "Synthesis of monopulse sub-arrayed linear and planar array antennas with optimized sidelobes," *Progress In Electromagnetics Research Letters*, Vol. 99, 109–129, 2009.
6. Yuan, T., N. Yuan, L. W. Li, and M.-S. Leong, "Design and analysis of phased anntena array with low sidelobe by fast algoritm," *Progress In Electromagnetics Research Letters*, Vol. 87, 131–147, 2008.
7. Vázquez, C., G. Hotopan, S. Ver Hoeye, M. Fernández, L. F. Herrán, and F. Las-Heras, "Microstrip antenna design based on stacked patches for reconfigurable two dimensional planar array topologies," *Progress In Electromagnetics Research*, Vol. 97, 95–104, 2009.
8. Ver Hoeye, S., C. Vázquez, M. Fernández, L. F. Herrán, and F. Las-Heras, "Receiving phased antenna array based on injection-locked harmonic self-oscillating mixers," *IEEE Transactions on Antennas and Propagation*, Vol. 57, 2009.
9. Li, G., S. Yang, Y. Chen, and Z. Nie, "A novel electronic beam steering technique in time modulated antenna arrays," *Progress In Electromagnetics Research*, Vol. 97, 391–405, 2009.
10. Ouyang, J., F. Yang, S. W. Yang, Z. P. Nie, and Z. Q. Zhao, "A novel radiation pattern and frequency reconfigurable microstrip

antenna on a thin substrate for wide-band and wide-angle scanning applications," *Progress In Electromagnetics Research Letters*, Vol. 4, 167–172, 2008.

11. Hall, L., H. Hansen, and D. Abbott, "Rotman lens for mm-wavelengths," *Proceedings of SPIE*, Vol. 4935, 2002.
12. Butler, J. and R. Lowe, "Beam forming matrix simplifies design of electronically scanned antennas," *IEEE Transactions on Applied Superconductivity*, 1961.
13. Ishimaru, A. and H.-S. Tuan, "Theory of frequency scanning antennas," *IRE Transactions on Antennas and Propagation*, 1962.
14. Spradley, J., "A volumetric electrically scanned two-dimensional microwave antenna array," *IRE International Convention Record*, 1958.
15. Lee, K. F. and W. Chen, *Advances in Microstrip and Printed Antennas,* John Wiley & Sons, inc., 1997.
16. Sawaya, K., H. Sato, Y. Wagatsuma, and K. Mizuno, "Broadband Fermi antenna and its application to mm-wave imaging," *European Conference on Antennas and Propagation*, 2007.
17. Lin, S., S. Yang, and A. E. Fathy, "Development of a novel UWB Vivaldi antenna array using SIW technology," *Progress In Electromagnetic Research*, Vol. 90, 369–384, 2009.
18. Wu, Y., Y. Liu, and S. Li, "Dual-band modified Wilkinson power divider without transmission line stubs and reactive components," *Progress In Electromagnetics Research*, Vol. 96, 9–20, 2009.
19. Wang, D., H. Zhang, T. Xu, H. Wang, and G. Zhang, "Design and optimization of equal split broadband microstrip Wilkinson power divider using enhanced particle swarm optimization algorithm," *Progress In Electromagnetics Research*, Vol. 118, 321–334, 2011.
20. Wu, Y., Y. Liu, and S. Li, "A new dual-frequency Wilkinson power divider," *Journal of Electromagnetic Waves and Applications*, Vol. 23, No. 4, 483–492, 2009.
21. Zhang, Z., Y.-C. Jiao, S. Tu, S.-M. Ning, and S.-F. Cao, "A miniaturized broadband 4:1 unequal Wilkinson power divider," *Journal of Electromagnetic Waves and Applications*, Vol. 24, No. 4, 505–511, 2010.